PAPER

Check for updates

Catalytic vapour phase hydrodehalogenation of 1,8-dichlorooctane over Pd@MIL-101(Cr)-NH$_2$: a step forward in MOF-based technologies

Raúl M. Guerrero, [a,b,c] Ignacio D. Lemir, [a,b] Carlos Fernández-Ruiz, [a,b] Sergio Carrasco, [a] Patricia Horcajada, [a] David P. Serrano, [b,d] Yolanda Pérez *[a,e] and Patricia Pizarro *[b,d]

Catalytic hydrodehalogenation (HDH) represents a promising strategy to remove halogens (Cl and Br) in pyrolysis oils derived from halogenated plastic waste. Metal–organic frameworks (MOFs) offer a potential alternative to conventional HDH catalysts due to their outstanding properties in terms of porosity and surface area, thus allowing better dispersion of active phases. In this work, a Pd@MOF catalyst is studied for the HDH of 1,8-dichlorooctane, selected as a model chlorinated organic compound, using a continuous fixed-bed reactor under vapor phase conditions. A first screening for MOFs with different structures and compositions evidenced a much better performance of those synthesized under microwave radiation (UiO-66-NH$_2$ and MIL-101(Cr)-NH$_2$) due to their smaller particle sizes that improved the surface-to-volume ratios and reduced diffusional restrictions. Among these two MOFs, MIL-101(Cr)-NH$_2$ was selected for the dispersion of Pd nanoparticles due to its superior catalytic stability over time on stream, as compared with UiO-66-NH$_2$. Using as a reference commercial catalyst (5 wt% Pd dispersed on Al$_2$O$_3$), a superior activity was observed over the Pd@MOF composite (100% conversion and almost full selectivity to *n*-octane after 4 h), which was attributed to the confinement of well-dispersed Pd nanoparticles within the MOF matrix, effectively preventing their agglomeration during the reaction, as confirmed by transmission electron microscopy (TEM) analysis. Through the combination of different characterization techniques such as active oxidative decomposition (AOD) combined with ion chromatography (IC), gas chromatography coupled with mass spectrometry (GC-MS), and X-ray photoelectron spectroscopy (XPS) analysis of the catalyst, we concluded that the released chlorine, from 1,8-dichlorooctane HDH, was mostly retained in the Pd@MOF catalyst. Interestingly, the composite was regenerated by *in situ* thermal desorption and reused keeping the initial activity for 12 h.

Green foundation

1. We employed a continuous fixed-bed reactor operating under vapor phase conditions for the hydrodehalogenation (HDH) of alkyl halides as a representative of halogenated compounds which could be generated from the thermochemical conversion of plastic waste. HDH not only facilitates the recycling of plastics but also reduces the formation of harmful by-products, offering a sustainable strategy for plastic waste valorization.

2. Using the synthesized Pd@MIL-101(Cr)-NH$_2$ catalyst, the HDH performance was significantly superior to that of the commercially available Pd@Al$_2$O$_3$ catalyst. The former exhibited nearly 100% selectivity towards octane and reduced Cl content from 1000 ppm to below 20 ppm (within industrial fuel standards), compared to 70% selectivity and 325 ppm for the latter. Notably, the high activity of the as-synthesized catalyst was maintained for the whole 12 h of reaction time tested (8 h of continuous operation + 4 h after *in situ* regeneration).

3. The catalyst showed promising applicability for the dehalogenation of real pyrolysis oils obtained from halogenated plastic waste.

[a]*Advanced Porous Materials Unit, IMDEA Energy Institute, Avda. Ramón de la Sagra, 3, Móstoles, 28935 Madrid, Spain. E-mail: yolanda.cortes@urjc.es, raul.mulero@imdea.org, ignacio.lemir@imdea.org, sergio.carrasco@imdea.org, david.serrano@imdea.org*
[b]*Thermochemical Processes Unit, IMDEA Energy Institute, Avda. Ramón de la Sagra, 3, Móstoles, 28935 Madrid, Spain. E-mail: patricia.pizarro@imdea.org*
[c]*Escuela Internacional de Doctorado, Rey Juan Carlos University, C/Tulipán, s/n, Móstoles, 28933 Madrid, Spain*
[d]*Chemical and Environmental Engineering Group, Rey Juan Carlos University, C/Tulipán, s/n, Móstoles, 28933 Madrid, Spain*
[e]*COMET-NANO Group, ESCET, Universidad Rey Juan Carlos, C/Tulipán, s/n, Móstoles, 28933 Madrid, Spain*

1 Introduction

Halogens are present in a variety of commonly used plastics, primarily as part of additives or within the polymer structure itself. Their presence poses several environmental and health issues,[1] especially when these plastics are managed at the end of their life cycle. This is of particular importance during chemical transformation *via* pyrolysis of halogenated plastic waste not suitable for mechanical recycling.[2] The resultant pyrolytic oils usually contain a variety of organic compounds and halogenated species (mainly Cl- and Br-containing components), requiring further upgrading treatments to meet specifications for valuable uses, such as in fuel formulations or chemical production. Typically, pyrolysis oils derived from halogenated plastic waste exhibit chlorine contents ranging from 500 to 1000 ppm, whereas levels above 20 ppm are unacceptable for petrochemical applications.[3–6] Moreover, several challenges need to be faced for the post-processing of halogenated oils, such as the potential formation of hydrogen halides, which cause corrosion of equipment, the formation of toxic compounds like dioxins or furans, and excessive energy consumption, thereby increasing the cost of treatment.[7–9]

In this context, research on catalytic hydrodehalogenation (HDH) has gained increasing importance because of its huge potential to be coupled in a cascade catalytic process for the valorization of halogenated plastic waste into valuable products.[10–12] In HDH reactions, metallic catalysts such as palladium,[13] nickel,[14] copper,[15] platinum,[15] and rhodium[16] have been commonly employed in the presence of hydrogen to promote the cleavage of carbon–halogen (C–X) bonds, reducing them to carbon–hydrogen (C–H) bonds with the subsequent removal of the halogen. This process not only enhances the recycling of plastics, but also reduces the formation of harmful by-products, being a sustainable approach for plastic waste valorization.

Current studies on HDH processes are centered on the reduction and recycling of precious metals as active phases, as well as on the development of catalyst supports that enhance the physicochemical properties of the resulting materials, thereby improving catalytic performance in terms of conversion and full dehalogenation capacity. Among all metals, palladium has traditionally been used as a reference in such reactions due to its high catalytic activity and strong reductive capacity. However, because of its high cost and limited availability, it is often used on commercially available supports, such as Pd/C and Pd/Al$_2$O$_3$,[17,18] with limited tunability of their textural properties.

In line with the emerging trends of employing active supports instead of inert materials, metal–organic frameworks (MOFs) have emerged as attractive and promising alternatives for their use as catalytic supports.[19–21] MOFs significantly surpass conventional supports (*e.g.*, carbon and alumina) in terms of porosity and surface area, which allow efficient dispersion of active phases, thereby maximizing their exposition to the reactive species.[22–25] Additionally, their compositional and structural versatility lead to a variety of interesting physicochemical properties, enabling a large extent of modifications.[26] For instance, different functional groups (–NH$_2$, COOH, *etc.*) can be introduced to stabilize nanometric metal colloids, facilitating their anchoring and preventing potential leaching of the active phase.[27] Additionally, encapsulation and spatial confinement effects, provided by the porous nature of MOFs, contribute to reducing poisoning, enhancing the stability of these composites and, sometimes, leading to a synergistic catalytic effect between the MOF matrix and the metal nanoparticle.[28] These aspects circumvent agglomeration and extend the lifespan of such composites, broadening their application scope.[29,30] In particular, composites of metallic nanoparticles and MOFs have been extensively studied in a wide range of catalytic applications, but reports on their direct application in HDH reactions are scarce.[31–34] In 2012, Huang *et al.*[35] reported the evaluation of a composite based on two Cr-MOFs as palladium supports (Pd@MIL-53 and Pd@MIL-101(Cr)-NH$_2$) for the HDH of a variety of aryl chlorides, using a liquid-phase batch reaction system and an aqueous solution of ammonium formate as a hydrogen source. Very high yields, between 91 and 98% of dehalogenated products, depending on the aryl chloride composition, were attained. Years later, Tong *et al.*[36] synthesized and evaluated Pd@UiO-66 in the HDH reaction, also focusing on halogenated aromatic compounds as substrates and achieving complete chlorine removal with 100% selectivity towards phenols. The main contribution provided by these authors lies in the development of a highly reactive material and the design of an aqueous methodology to promote HDH. However, there are no reported studies on MOF-based catalyzed HDH reactions using alkyl halides, which could lead to valuable molecules, such as hydrocarbon for liquid fuel production. Furthermore, the abovementioned studies were all carried out in liquid-phase batch reactors, with remaining unexplored fixed-bed reactors under vapor phase conditions, which could provide important insights about continuous operation modes and catalyst deactivation.

In this context, we evaluate for the first time a composite based on Pd nanoparticles and MOFs (Pd@MOF) as a HDH catalyst in a continuous flow fixed-bed reaction system operating under vapor-phase conditions, in contrast to previous studies performed in liquid-phase batch reactors. 1,8-Dichlorooctane was selected as a model molecule to represent halogenated organics which could be formed from plastic waste pyrolysis.[37] Concerning the catalytic supports, four MOFs with different structures and compositions were selected exhibiting high porosity (see Table S1), ability to adsorb the alkyl substrate *a priori*, and high thermal stability, compatible with the HDH conditions (265 °C under H$_2$/N$_2$): (i) the mesoporous chromium(III) aminoterephthalate MIL-101(Cr)-NH$_2$ (2344 m^2 g^{-1}, pore size = 21 and 26 Å, accessible through microporous windows of 12 and 14 Å; thermal stability = 280 °C);[38] (ii) mesoporous aluminum(III) trimesate MIL-100(Al) (1539 m^2 g^{-1}, pore size = 20 and 24 Å, accessible through microporous windows of 8 and 11 Å; thermal stability = 450 °C);[39] (iii) mesoporous zirconium(IV) tetrakis(*p*-benzoate)

pyrene NU-1000 (1778 m^2 g^{-1}, pore size = 23 and 35 Å; accessible *via* 14 Å windows; thermal stability = 400 °C);[40] and (iv) the microporous zirconium(IV) aminoterephthalate UiO-66-NH$_2$ (1035 m^2 g^{-1}, pore size = 13 Å, accessible through triangular apertures of 7 Å; thermal stability = 410 °C).[41] Furthermore, an in-depth analytical study was conducted to establish an accurate Cl mass balance, with particular emphasis on identifying and detecting chlorinated species formed during the reaction. Considering the above statements, this work highlights the first use of MOF-based materials as a competitive class of catalytic supports for HDH under continuous-flow conditions. Our findings show their structural robustness, ability to stabilize Pd nanoparticles, and effective performance under vapor-phase operation over hours-on-stream. These results pave the way for designing metal–MOF systems for detoxifying complex halogenated streams from plastic waste valorization, advancing scalable and sustainable purification technologies.

2 Materials and methods

2.1 Synthesis of catalysts

Synthesis of MOFs. Most MOFs used as catalysts in this work were synthesized using previously reported methods: MIL-100(Al),[39] NU-1000,[40] and UiO-66-NH$_2$,[41] except MIL-101(Cr)-NH$_2$, whose preparation was slightly modified as described below.

Synthesis of MIL-101(Cr)-NH$_2$. The synthesis of MIL-101(Cr)-NH$_2$ was done using a multimodal microwave instrument (MMW, One Touch Technology Mars6 240/50) following a method reported in the literature with slight modifications.[38] In this way, Cr(NO$_3$)$_3$·9H$_2$O (600 mg; 1.5 mmol), 2-ATA (272 mg; 1.5 mmol), and KF (236 mg; 4.71 mmol, used with protection under fume hood in accordance with the Safety Data Sheet guidelines) were dissolved in 15 mL of Milli-Q water inside a 45 mL microwave Teflon-lined reactor. The mixture was sonicated in the Teflon-lined reactor for a few minutes, and then, magnetically stirred for 20 min. Subsequently, the reactor was placed in a microwave oven, and subjected to the following program: (i) heating from room temperature to 175 °C, within 5 min; (ii) maintaining 175 °C for 1 h (max. pressure: 14.0 bar, 15–20 W); and (iii) cooling down to 60 °C, within 10 min under an airflow. The resulting green suspension was washed with absolute ethanol (15 mL) and Milli-Q water (15 mL) in a 50 mL plastic tube followed by centrifugation (3×, 11 500 rpm, 10 min). This was repeated three times with fresh absolute ethanol (30 mL) under similar centrifugation conditions. The material was dried at 100 °C for 12 h, obtaining a green powder (793 mg; 70 ± 4% yield (*n* = 4) on metal basis considering a molecular weight of the MOF of 764.40 g mol^{-1}). The space–time yield (STY) was estimated to be 1268 kg m^{-3} day^{-1}.

Synthesis of Pd@MIL-101(Cr)-NH$_2$. To prepare Pd nanoparticles in MIL-101(Cr)-NH$_2$, our previous protocol for the synthesis of Pd@UiO-66-NH$_2$ in multimodal microwave (MMW) was adapted,[41] which includes the wet impregnation of the metal precursor followed by an *in situ* chemical reduction of the palladium salt. Briefly, the microwave (MMW)-prepared MIL-101(Cr)-NH$_2$ (100 mg, 0.13 mmol) and PdCl$_2$ were mixed (5 wt% theoretical Pd loading) in 10 mL of Milli-Q water and stirred for 30 min in a Teflon-lined reactor. Subsequently, 1 mL of a NaBH$_4$ solution (3 mg mL^{-1} in MeOH) was added dropwise under vigorous stirring for 20 min. The protocol included: (i) heating from 25 to 150 °C in 5 min, (ii) maintaining 150 °C for 10 min (15–20 W), and (iii) cooling to 60 °C using air. The composite was recovered by filtration (nylon, 0.22 μm) and washed repeatedly with deionized water.

2.2 Hydrodehalogenation (HDH) reaction tests

The HDH activity of the synthesized materials was evaluated in the vapor phase using a model feed of 1,8-dichlorooctane (1000 ppm of Cl) diluted in *n*-decane. The reaction system was a down-flow stainless steel fixed-bed reactor (diameter of 1/2, length: 25 mm), as illustrated in Fig. 1.

This HDH system consists of two main sections: the upper part, where the catalytic bed is located and the hydrodechlorination reaction occurs, and the lower part, where the reaction products are condensed to collect the treated oil.

In a typical reaction, 270 mg of a catalyst is introduced into the catalytic bed at a suitable height using a stainless-steel tube, grids, and glass wool. Subsequently, the system is purged with a N$_2$ flow with a mass flow controller (Bronkhorst El-Flow). After the purge and just before starting the reaction, the gas flow is switched to a mixture of H$_2$ + N$_2$ (25 mL min^{-1} H$_2$ and 25 mL min^{-1} N$_2$). At the same time, the temperature of the catalytic bed (regulated by using a type K thermocouple) gradually reaches 265 °C (4 °C min^{-1} heating ramp). By means of a back-pressure regulator (BPR), the reaction pressure is set at 5 bar. Once the system is fully prepared to initiate the reaction, the feed mixture is pumped by using an HPLC pump (0.2 mL min^{-1}) to the top of the reactor where it mixes with the H$_2$ and N$_2$ flow and vaporizes in the reactor inlet. The vaporized feed goes through the catalytic bed where the halogen is selectively removed *via* the HDH reaction. At the exit of the reactor, the heavier compounds are condensed using ice bags at 0 °C (fraction denoted as treated oil). Then, the non-condensed gas stream passes through various bubblers at 0 °C containing a 0.1 M Na$_2$CO$_3$ solution to capture any HCl generated during the process. The remaining gaseous products not captured in the previous stages pass through a totalizer to measure the volume of gas produced during the reaction and are finally collected in inert plastic bags for analysis. The reaction is maintained up to 4 h (treating 7 g h^{-1} feed). The condensed products and gas sampling bags are collected at the end of every hour for their analysis. Absolute errors were determined by the repetition of reactions under identical operating conditions (see the SI for further information).

Recyclability tests were performed using the most active catalyst, and successive reactions of 4 h were carried out. In total, two consecutive 4-hour cycles were conducted, amount-
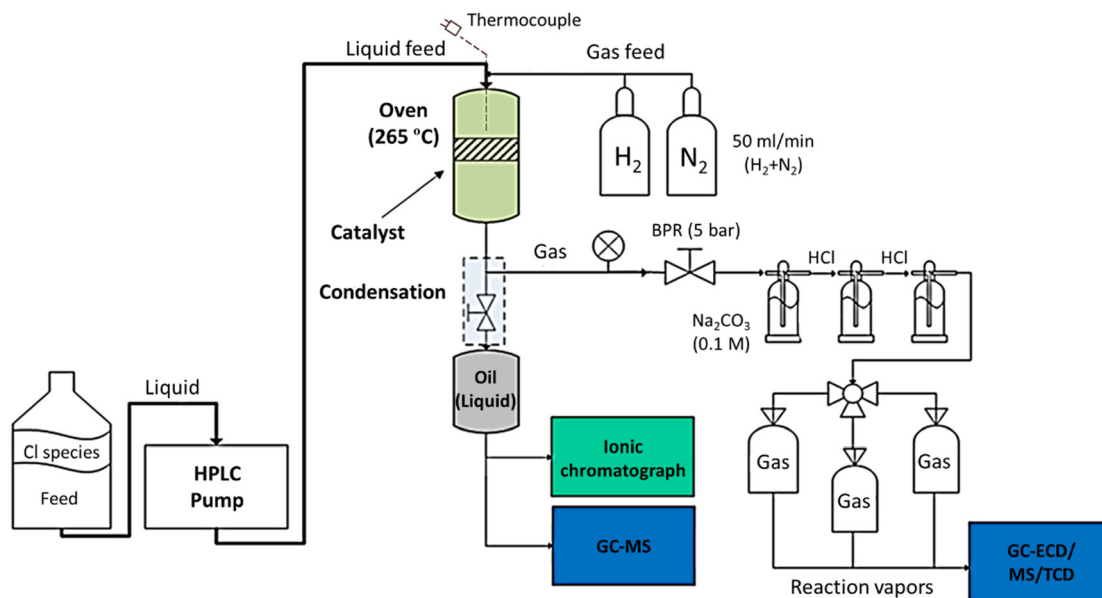
Fig. 1 Experimental setup for the catalytic HDH experiments.

ing to 8 hours of continuous operation under identical reaction conditions. Finally, the reused catalyst underwent an *in situ* regeneration process. After 8 h of reaction, the catalyst was maintained at the reaction temperature under a continuous flow of H_2 and N_2 for 3 h. This treatment facilitated the desorption of the adsorbed species, the cleaning of the catalyst surface, and its reactivation. The regenerated material was tested in the subsequent reactions to assess its HDH activity and catalytic performances.

3   Results and discussion

3.1   Screening of MOFs in the hydrodehalogenation (HDH) reaction

The four selected highly porous MOFs were synthesized by either solvothermal (NU-1000 and MIL-100(Al)) or microwave-assisted methods (UiO-66-NH$_2$ and MIL-101(Cr)-NH$_2$) and fully characterized (PXRD, FTIR, TGA and N_2 sorption), confirming their structural, compositional and textural properties, in agreement with the previous reports (see Fig. S1–S3 and Table S1).[41–44] Note here that TGA in air revealed that the prepared MOFs had decomposition temperatures above 300 °C (Fig. S4 and S5), which was consistent with the previously reported values.[39–41] However, MIL-101(Cr)-NH$_2$ showed slightly lower stability compared to those reported in the literature (280 *vs.* 320–350 °C).[38,42] This difference could be attributed to the presence of both a small amount of released fluoride ions, acting as fluxes,[45] and defects within the network, as reported elsewhere.[41]

While fluoride incorporation can enhance MOF catalytic performance or modify structural features to improve active site accessibility,[46,47] it may adversely affect thermal stability.

Fluorine can form stable compounds with metal cations (*e.g.* chromium fluoride) or act as a counteranion (*e.g.* $NH_3^+F^-$), compromising the integrity of the MOF's coordination framework (further details in the XPS section below). In addition, it can decrease the melting point and facilitate side reactions, potentially leading to the structure collapse at lower temperatures than that expected for pristine MIL-101(Cr)-NH$_2$.[48,49] Additionally, N_2 adsorption–desorption isotherms (see Fig. S3 and Table S1) showed that the BET surface area (S_{BET}, 2344 m^2 g^{-1}) was in the range of the reported values. However, the pore volume (V_{PORE}, 1.24 cm^3 g^{-1}) was relatively smaller than expected (1.63 cm^3 g^{-1}),[50] possibly because of incorporating F$^-$ into the framework, this effect being especially notable in the case of aminated polymers, as we have already reported elsewhere.[38] The modulator KF stabilizes the Cr$_3$O nodes through the coordination of F$^-$ ions, which act as charge-balancing ligands. Finally, the thermal stability of MIL-101(Cr)-NH$_2$ was also examined by TGA under an inert atmosphere (Ar) (Fig. S6). Here, we observed that degradation occurred above 300 °C, indicating the preservation of its stability at the HDH reaction temperature (265 °C).

In the initial approach, the four selected MOFs were screened and compared as catalysts for the HDH reaction of 1,8-dichlorooctane in *n*-decane corresponding to a Cl content in the feedstock of 1000 ppm. The weight hourly space velocity (WHSV) for the reaction was 0.38 h^{-1}, indicating the amount of reactant (1,8-dichlorooctane) fed per hour and per gram of catalyst. Fig. 2 shows the reaction results in terms of conversion, selectivity and HDH degree for all materials tested after 1 h of reaction at 265 °C and with an equimolar flow of N_2 + H_2. In addition, a thermal blank reaction was carried out in the absence of a catalyst as reference, corroborating a null conversion of 1,8-dichlorooctane.
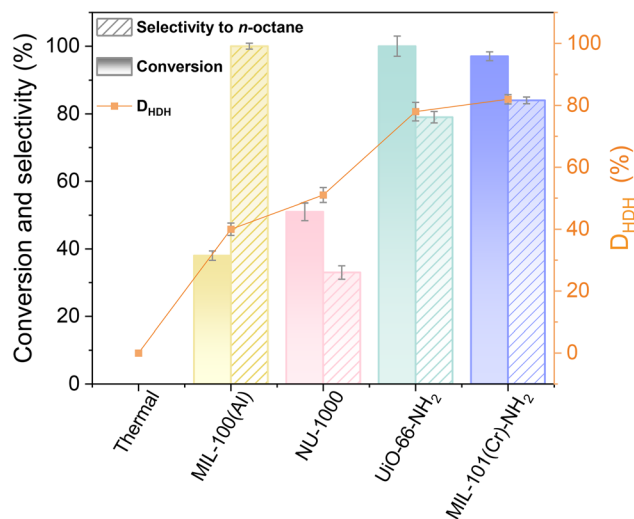
Fig. 2 Catalytic HDH of 1,8-dichloroctane: conversion/selectivity (plain/striped bars, respectively) and HDH degree (D_{HDH}) over different MOF catalysts: MIL-100(Al), NU-1000, UiO-66-NH$_2$, and MIL-101(Cr)-NH$_2$. Reaction conditions: 265 °C, equimolar flow of N$_2$ + H$_2$, 1 h, 0.38 h^{-1}.

A clear difference of activity was observed depending on the type of MOF used as a catalyst. Specifically, those obtained through solvothermal methods (MIL-100(Al) and NU-1000) exhibited lower activity, with conversions of 38 and 51%, respectively, and D_{HDH} capacities below 55% in both cases. In contrast, those MOFs synthesized under microwave radiation (UiO-66-NH$_2$ and MIL-101(Cr)-NH$_2$) led to an almost complete conversion (Fig. 2, green and blue) and HDH degrees of up to 82% in only 1 h. This significantly higher performance is attributed to a reduction of the MOF particle size to the nanometric scale and the creation of defects (*i.e.* improving accessibility of the chloride-containing compound to metal active sites) by microwave methodologies in contrast to the typical solvothermal synthesis methods.[51] Indeed, MIL-101(Cr)-NH$_2$, prepared here under a new microwave method, showed a significant reduction in particle size compared to other methodologies, as confirmed by transmission electron microscopy (TEM, Fig. S7a). The obtained crystals exhibited a well-defined octahedral morphology with sizes of 30 ± 8 nm. In comparison, previously reported syntheses using monomodal microwave and solvothermal methods yielded considerably larger particles, with sizes of around 80 nm and 300 nm, respectively.[38,52] On the other hand, while UiO-66-NH$_2$ exhibited a comparable particle size of 28 ± 3 nm, MIL-100(Al) and NU-1000 were considerably larger, with sizes of 650 ± 110 nm and 1.6 ± 0.7 μm, respectively (see Fig. S7b–d). These results highlight the efficiency of our adapted synthesis to produce small particle sizes with enhanced catalytic activity. By controlling different synthetic parameters that affect polydispersity, nucleation can be favored over crystal growth, resulting in reduced particle sizes, as previously stated. Thus, these nanometric MOFs result in (i) higher surface-to-volume ratios,

exposing a greater number of active sites that are essential for facilitating catalytic reactions, and (ii) improved diffusion kinetics of the reactant due to shorter inner path lengths.

In summary, both MMW-derived MOFs showed a high D_{HDH} capacity: 78% for UiO-66-NH$_2$ and 82% for MIL-101(Cr)-NH$_2$. Although UiO-66-NH$_2$ achieves 100% conversion, it does not fully eliminate the chlorine in the treated oil. Thus, *n*-octane is the major product (79%), but the remaining 21% corresponds to 1-chlorooctane. This partially dehalogenated by-product accounts for a total Cl content of 211 ppm in the oil. On the other hand, although MIL-101(Cr)-NH$_2$ exhibits a slightly lower conversion (97%), its selectivity towards the fully dehalogenated compound (*n*-octane) is higher, with a selectivity of 84%. Thus, MIL-101(Cr)-NH$_2$ shows an excellent capacity to remove chlorine from the halogenated substrate. As a result, the oil treated with this MOF contains the lowest amount of chlorine (184 ppm, in the form of 1,8-dichlorooctane and 1-chlorooctane).

3.2 HDH reaction using MIL-101(Cr)-NH$_2$ and UiO-66-NH$_2$ catalysts

After identifying the two most promising catalysts, the reaction time was extended from 1 to 4 h to evaluate their performance along the time on stream and determine which material has greater potential for future studies (Fig. 3 and Table S2). While both MOFs exhibited similar activities during the first hour of reaction, UiO-66-NH$_2$ suffered a progressive decrease both in conversion and selectivity to *n*-octane during the following 3 h, reaching values of 69% and 56%, respectively. This material was unable to achieve complete dehalogenation of the initial molecule, 1,8-dichlorooctane, predominantly producing the intermediate by-product, 1-chlorooctane (75%), by the end of the reaction. In contrast, MIL-101(Cr)-NH$_2$ maintained a conversion of nearly 100% and about 90% selectivity towards
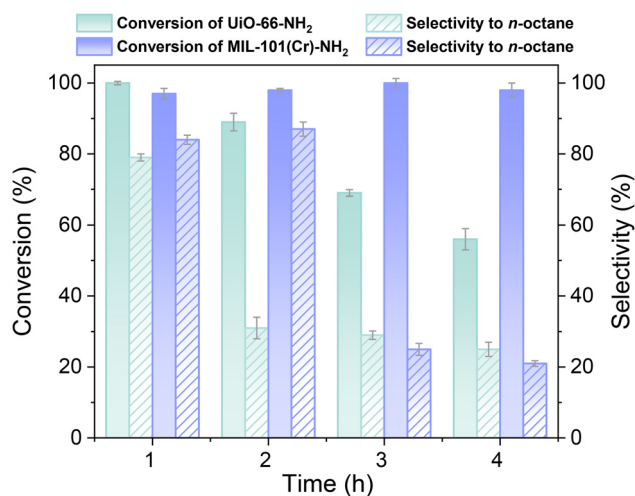

Fig. 3 Catalytic HDH of 1,8-dichloroctane: conversion and selectivity to *n*-octane obtained over UiO-66-NH$_2$ and MIL-101(Cr)-NH$_2$ catalysts during 4 h of time on stream. Reaction conditions: 265 °C, equimolar flow of N$_2$ + H$_2$, 0.38 h^{-1}.

n-octane, achieving almost complete hydrodechlorination of the treated oil after 2 h. Longer reaction times did not significantly affect the conversion but led to a decrease in the HDH capacity, with the selectivity to n-octane becoming comparable to that of UiO-66-NH$_2$. Both MOF catalysts were analyzed by TEM and XRD techniques to check their structural stability after 4 h of reaction. TEM (Fig. S8) images revealed partial agglomeration of the MOF nanoparticles in both cases. XRD (Fig. S9) patterns confirmed the preservation of the crystalline structure, although a peak-broadening effect was observed, more severe in the case of UiO-66-NH$_2$ and consistent with a different pore content and/or partial amorphization.

The difference in catalytic activity between MIL-101(Cr)-NH$_2$ and UiO-66-NH$_2$ can be attributed to a number of parameters, such as their distinct textural properties, the Lewis acidity strength of the metal centers, the Brønsted acidity of –OH bridges, the presence of fluoride atoms, and/or the possible defects generated during microwave-assisted synthesis[53–56] (see Table S3). Note here that: (i) MIL-101(Cr)-NH$_2$ has a significantly higher BET surface area than UiO-66-NH$_2$ (2344 vs. 1034 m^2 g^{-1}), which means more availability of active sites and better interaction with reactants; (ii) the pore volume of MIL-101(Cr)-NH$_2$ is also notably larger (1.24 vs. 0.34 cm^3 g^{-1}), enhancing the diffusion of reactants within the material and accelerating the removal of products, both being critical factors for good catalytic performance; (iii) although the metal ion (Zr^{4+}) in UiO-66-NH$_2$ exhibits stronger Lewis acidity than the metal ion (Cr^{3+}) in MIL-101(Cr)-NH$_2$, the presence of fluoride in the latter can enhance its catalytic activity, since fluoride groups increase the acidity of the metal active sites,[57] making them more effective in promoting catalytic reactions; and (iv) the highest concentration of defects in MIL-101(Cr)-NH$_2$ (33% vs. 20% missing linkers for MIL-101(Cr)-NH$_2$ and UiO-66-NH$_2$, estimated by TGA, see the SI),[58,59] which is one of the key factors to explain the better performance of MIL-101(Cr)-NH$_2$, since these defects create additional active sites, improving the material's ability to interact with the reactants.[60,61] Thus, the missing linker defects result in a higher density of coordinatively unsaturated sites (CUS) in MIL-101(Cr)-NH$_2$, which serve as additional active centers for the adsorption and activation of chlorinated compounds, significantly enhancing its catalytic efficiency compared to UiO-66-NH$_2$.

It is crucial to emphasize that, in comparison with other studies in vapor phase, where catalysts are MOF-derived metal–carbon composite materials, MIL-101(Cr)-NH$_2$ emerges as a significantly more effective catalyst for the HDH of alkyl halides. For example, as reported by Ning et al.,[62] with Ni-MOF-74-derived catalysts, after undergoing pyrolysis and carbonization, the material achieved a maximum conversion of only 70% in the hydrodechlorination reaction of 1,2-dichloroethane. In contrast, MIL-101(Cr)-NH$_2$ achieved an outstanding conversion, showing that MOFs can serve as efficient catalysts in their pristine form, without requiring thermal degradation to oxides or carbon composites. According to the catalytic results and the characterization analysis, MIL-101(Cr)-NH$_2$ was selected as the most promising catalyst for a more in-depth study.

3.3 HDH reaction using the Pd@MIL-101(Cr)-NH$_2$ composite

MOF MIL-101(Cr)-NH$_2$ was loaded with Pd(II) in order to enhance its HDH performance. Imbibed cations were rapidly reduced in a further step via microwave radiation in the presence of NaBH$_4$ as a reducing agent, following our previously reported method.[41] While the theoretical Pd content was 5 wt%, the actual loading determined by ICP-OES was 4.3 ± 0.2 wt%. This deviation was attributed to minor losses of Pd cations during the impregnation step, a common occurrence in wet impregnation protocols. XRD analysis revealed that the structure remained unaltered after Pd loading and reduction (Fig. S10a). On the other hand, the absence of characteristic palladium peaks at 2θ = 40°, corresponding to the (111) plane, suggested the formation of small and well-dispersed Pd nanoparticles within the MOF porosity/framework (<4 nm).[63] To assess the thermal stability of the Pd(4.3%)@MIL-101(Cr)-NH$_2$ composite, variable-temperature X-ray diffraction (VT-XRD) analysis was performed. This technique was chosen to monitor the structural integrity of the MOF, as well as to observe the behavior and evolution of the Pd nanoparticles (Pd NPs) within the material at increasing temperatures (from 30 to 370 °C) under an inert atmosphere (Fig. S10b). In the plot, the green spectrum represents the crystallinity of the composite at 270 °C, close to the reaction temperature (265 °C), showing that the material remained unaltered, in agreement with the TGA (Fig. S6), indicating that the reaction environment does not affect the stability of the composite, further supporting the observed thermal behavior. Above 300 °C, a significant loss in crystallinity was observed as the organic part partially decomposed, allowing Pd NPs to agglomerate as deduced from the increase in the intensity of the peak at 40°.

TEM images (Fig. 4c and d) indicated that the morphology of the MIL-101(Cr)-NH$_2$ crystals remained unchanged after the
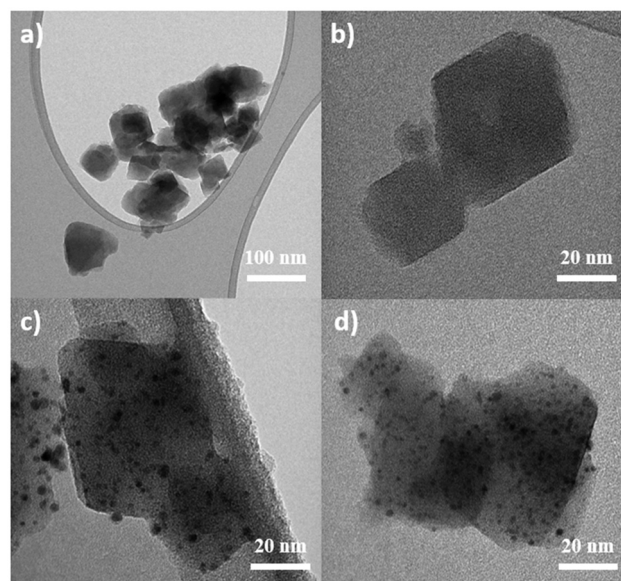

Fig. 4 TEM images of the pristine MOF MIL-101(Cr)-NH$_2$ (a and b) and the composite Pd@MIL-101(Cr)-NH$_2$ (c and d).

in situ reduction of the Pd NPs (as single sites and nano-clusters).[64] The Pd NPs were finely and homogeneously distributed within the MOF matrix, as confirmed by the mapping analysis (Fig. S11), with a mean size of 2.3 ± 0.6 nm (see the histogram in Fig. S12). Note that the diffraction limit in conventional diffractometers (Cu K-α) for Pd NPs is 2–3 nm,[63] supporting the absence of diffraction peaks in Fig. S10a and the particle size found herein. Also, after Pd loading, the textural properties exhibited a noticeable decrease (Fig. S13 and Table S4), with a reduction in the surface area $S_{BET} = 1391$ m^2 g^{-1} (Fig. S13a) and pore volume across the different pore types (Fig. S13b), which can be attributed either to the incorporation of Pd NPs within the MOF matrix and/or onto its external surface, hampering the accessibility of the gas probe during sorption measurements.

Finally, the oxidation states of the elements comprising the catalysts, MIL-101(Cr)-NH$_2$ and Pd@MIL-101(Cr)-NH$_2$, were analyzed by X-ray photoelectron spectroscopy (XPS). The survey spectra in Fig. 5a display the main elements (Cr, O, N, and C) corresponding to the primary components of the MOF. The Pd 3d signal was observed exclusively in the Pd@MIL-101(Cr)-NH$_2$ composite and could be deconvoluted into four peaks (see Fig. 5c). The two most intense Pd 3d$_{5/2}$ and Pd 3d$_{3/2}$ peaks at 337 and 343 eV corresponded to the formation of Pd^0,[41,65] while the two smaller peaks at 338 and 344 eV were ascribed to Pd^{2+}. This confirmed the formation of Pd^0 nanoparticles and suggested a slight surface reoxidation process of the Pd NPs under ambient conditions.[66] However, this is not a significant issue, since during the HDH reaction (H$_2$, 265 °C), which takes place in the presence of H$_2$, any residual Pd^{2+} is expected to be fully reduced to Pd^0, ensuring a proper formation of active nanoparticles for catalysis. Additionally, the N 1s peak, present in both the MOF and the composite, Fig. 5b, shows notable differences. Firstly, the peak in the composite is slightly shifted to higher binding energy values (400 eV) compared to that of the parent MOF (398 eV), suggesting a change from the electron density by possible interactions between the amine groups (–NH$_2$) of the MOF ligand and the Pd NPs.[67] Moreover, in the case of the parent MOF sample, the N 1s signal can be deconvoluted into two peaks: a more intense one corresponding to the –NH$_2$ groups and a weaker one corresponding to the ammonium ions (–NH$_3^+$). As mentioned above, this
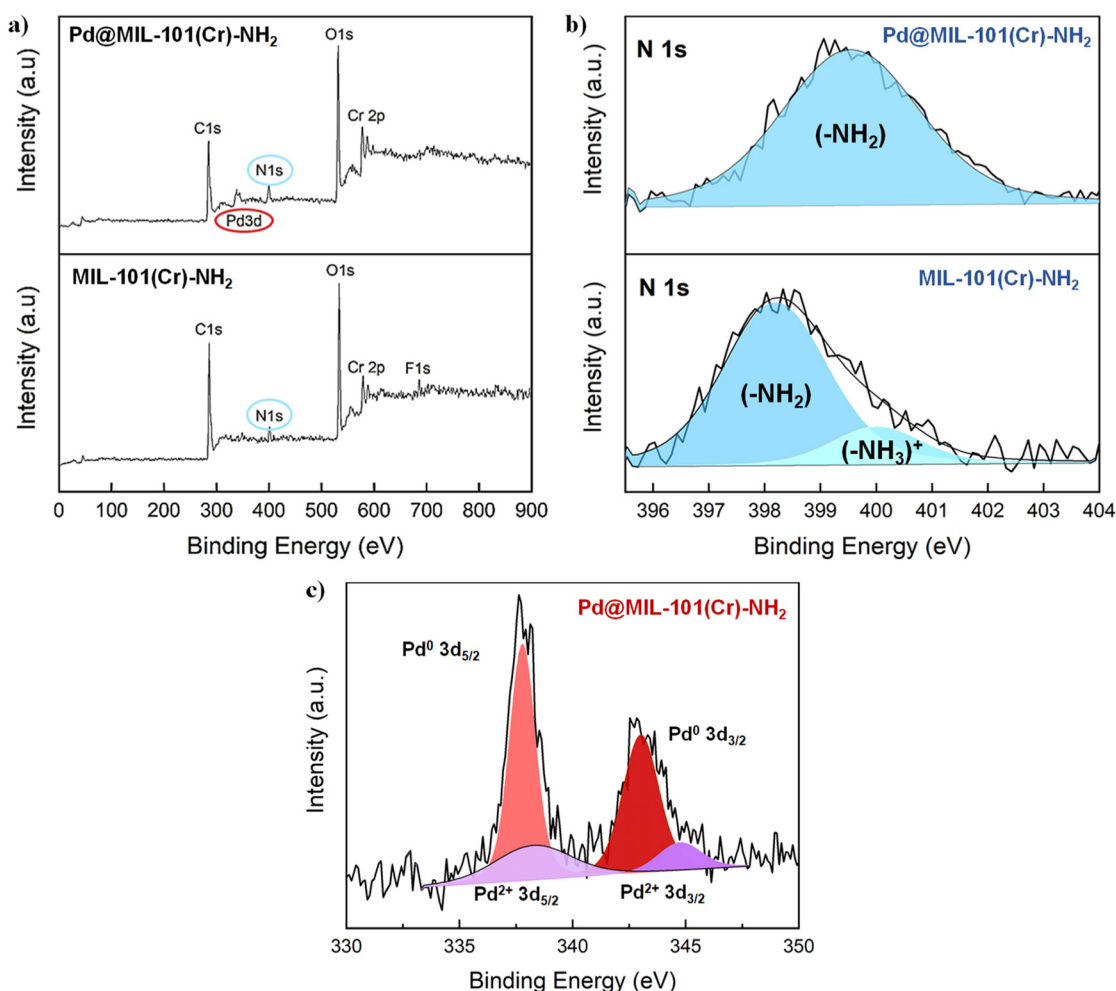

Fig. 5 XPS spectra of MIL-101(Cr)-NH$_2$ and Pd@MIL-101(Cr)-NH$_2$: (a) survey, (b) N1s region and (c) Pd 3d regions.

could be ascribed to the use of KF as a modulator during the MOF synthesis, resulting in a substantial amount of fluoride ion species (also observed in the MOF survey, F1s) being retained in the ammonium ions. However, after the composite synthesis, the F1s peak completely disappeared (Fig. 5a), and only the band corresponding to the –NH₂ groups was observed, indicating that the Pd incorporation process successfully removed any trace of the halogen.

The HDH performance of Pd(4.3%)@MIL-101(Cr)-NH₂ was evaluated and compared to the commercial Pd(5%)/Al₂O₃ catalyst, used here as the reference. Fig. 6a compares the results along 4 h of the reaction in terms of conversion and selectivity to *n*-octane. As can be observed, the MOF composite exhibited an excellent performance, with a very stable conversion of 100% during 4 h.

In comparison, the commercial catalyst also achieved notable conversions under similar reaction conditions, but slightly lower. The most significant difference lied in the selectivity to dechlorinated products: while the commercial

catalyst reached values close to 70% *n*-octane selectivity, Pd (4.3%)@MIL-101(Cr)-NH₂ maintained this parameter close to 100%. Regarding the D_{HDH} degree, Fig. 6b shows that during the first hour of the reaction, the composite achieved 100% HDH, resulting in a null chlorine concentration in the treated oil. In contrast, the oil treated with the commercial catalyst contained 325 ppm. After 4 h of reaction time, the composite maintained chlorine levels in the treated oil below 20 ppm, significantly outperforming the commercial catalyst.

During the reaction with the commercial catalyst, Pd(5%)/ Al₂O₃, Pd NPs tended to agglomerate and grow, reducing their catalytic activity (see Fig. S14b). In contrast, the MOF composite not only showed intrinsic active species in their metal centers, but also possessed a high specific surface area and porosity, providing a matrix to confine and protect Pd NPs. These aspects allowed for better dispersion and a more controlled growth of Pd nanoparticles, preventing their aggregation and thereby enhancing the catalytic activity of the MOF material in an effective manner (Fig. S14c).

Given the scarce literature on MOF-based catalysts under vapor-phase HDH in continuous flow, additional comparisons were made with other carbon-supported Pd systems (Pd/C, Pd/ CS, and Pd–Au/C), which share similarities with the commercial Pd/Al₂O₃ used as a benchmark in this study. In this context, it is noteworthy that the Pd/C catalyst prepared by Liu S. *et al.*[68] showed a good conversion for the HDH of dichloromethane. However, even under extended operation, the selectivity towards the fully dehalogenated product (methane) remained around 78%, with the formation of by-products such as ethane (C₂H₆), propane (C₃H₈), and methylchloromethane (MCM). On the other hand, the Pd/CS catalysts (Pd supported on CeO₂–Sm₂O₃) synthesized by Arevalo-Bastante *et al.*[69] for the dehalogenation of trichloromethane and dichloromethane achieved low rates of conversions of 50 and 60% even during high time on stream operations, with selectivities around 80 and 38% for methane, respectively. This highlights the limitations of these catalytic systems in sustaining high catalytic efficiency over time, making them less suitable for long-term HDH applications. Furthermore, other studies conducted under mild reaction conditions, even employing bimetallic catalysts, often fail to provide remarkable selectivity values, limiting their viability for sustainable fuel production. For instance, Bonarowska *et al.*[70] reported that a Pd–Au/C catalyst used for the hydrodechlorination of tetrachloromethane achieved high conversion values of 90%, but only with a 17% selectivity towards fully dehalogenated products. In contrast, our Pd@MIL-101(Cr)-NH₂ system not only achieved exceptional conversion and nearly complete selectivity, but also maintained a long-term performance under realistic HDH conditions. In this regard, it is important to highlight that the model feed employed in this study contains 1000 ppm of chlorine, a concentration that reflects the typical halogen content found in pyrolysis oils derived from halogenated plastic waste such as municipal residues or end-of-life vehicle (ELV) plastics. Typical values range from 500 to 1000 ppm,[3,4] whereas values above 20 ppm are unacceptable for its use in petrochemical plants.[5,6] Thus, the use of 1000 ppm Cl provides a techni-
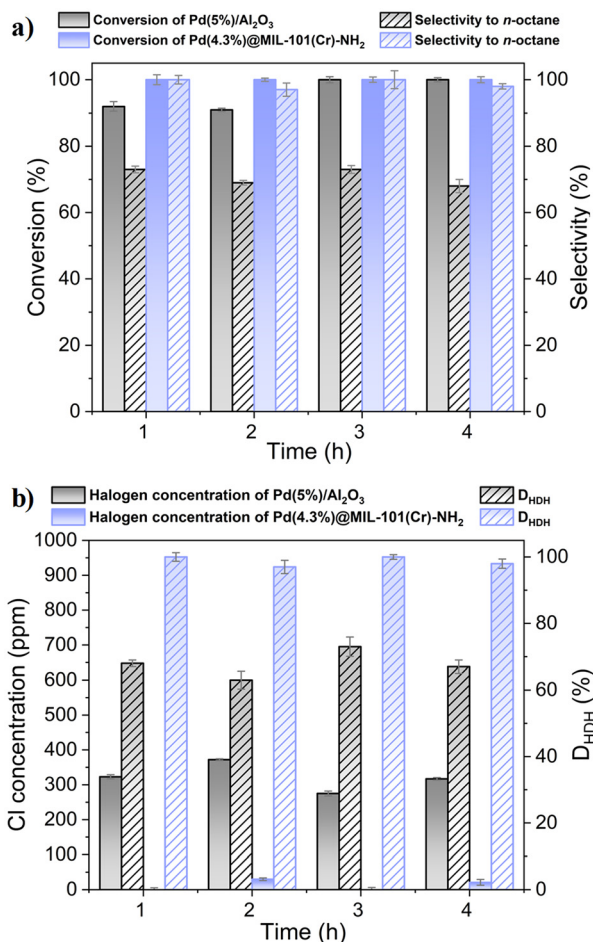

Fig. 6 Catalytic HDH of 1,8-dichloroctane: evolution with time of (a) conversion and selectivity to *n*-octane and (b) Cl concentration in the treated oil and HDH degree, for the catalysts Pd(5%)/Al₂O₃ and Pd(4.3%) @MIL-101(Cr)-NH₂. Reaction conditions: 265 °C, equimolar flow of N₂ + H₂, 0.38 h⁻¹.

cally relevant and representative benchmark for evaluating HDH catalyst performance, especially in terms of stability, activity, and selectivity under challenging but industrially realistic conditions. According to these results, the Pd@MIL-101(Cr)-NH$_2$ catalyst showed not only outstanding catalytic efficiency and robustness, but also clear potential for application in the upgrading of halogenated pyrolysis oils toward cleaner fuel production.

3.4 Oil dehalogenation, halogen distribution, and mechanism

In order to verify the closure of the overall mass chlorine balance and to assess how it is distributed in the different fractions attained after the hydrodechlorination reaction, the gaseous, liquid, and solid fractions were analyzed for the catalytic tests carried out with MIL-101(Cr)-NH$_2$ and Pd@MIL-101(Cr)-NH$_2$ using the model feed corresponding to 1000 ppm of Cl.

In the case of the gas fraction, it was collected during the 4-hour reaction period and analyzed by GC-ECD, but no chlorinated species were detected. In a similar way, the aqueous solution taken from the bubblers, where chlorine released during the reaction should be retained as HCl, typically showed minimal detectable amounts of chlorine by IC. The treated oils, as discussed in the previous sections, showed that the MOF and the Pd@MIL-101(Cr)-NH$_2$ composite had excellent HDH capacity, with low amounts of chlorine detected in this fraction of the product. Thus, the only remaining component where Cl could be accumulated was the used catalyst. As reported in other studies,[4,71] the catalyst with a high dehalogenation capacity can act also as a trap, capturing the produced chlorides and preventing them from being transported to the bubbler or reaching the gas bags. This result was confirmed through the XPS and TG/DTG analyses of the used catalyst (see Fig. 7 and Fig. S15).

Comparing the fresh and used catalyst, XPS spectral survey of the composite material after 4 h reaction time (Fig. 7a) exhibited Cl 2s and Cl 2p signals, indicating the presence of Cl species in the material. Moreover, analyzing the N 1S region for the fresh catalyst (Fig. 7b), only the peak corresponding to –NH$_2$ groups could be observed in the fresh composite. However, after the HDH reaction, the N 1s signal could be deconvoluted into two peaks (Fig. 7b), assigned to the –NH$_2$ and NH$_3^+$ groups, suggesting that the HCl formed in the reaction could be retained by the MOF ligand (–NH$_3^+$Cl$^-$). In fact, by washing the used catalyst with THF, a significant amount of halogen was desorbed (0.15 mg Cl g^{-1} feed for MIL-101(Cr)-NH$_2$ and 0.27 mg Cl g^{-1} feed for Pd@MIL-101(Cr)-NH$_2$). Further analysis of the washed THF by IC, together with the AOD + IC analyses of the washed catalyst, enabled the quantification of most of the Cl$^-$ generated during the reaction, resulting in a chlorine mass balance closure exceeding 94% in all cases. Regarding the XPS spectra of the Pd 3d region, the signal corresponding to Pd^{2+} of the fresh catalyst was completely absent after the HDH reaction (see Fig. S16) due to the pre-reaction conditioning process, where Pd in the MOF was fully reduced to Pd^0 under N$_2$ + H$_2$ flow at elevated temperatures, ensuring complete reduction of Pd before the reaction. During the catalytic test, reductive conditions were also maintained, avoiding Pd reoxidation.

The data obtained from the XPS analyses supported the interaction between chlorine and the composite. This insight not only provided a detailed understanding of the composite and its structural changes, but also allowed for the development of advanced methods to recover halogens and recycle the catalyst, thereby extending its reusability. Moreover, XPS was demonstrated to be a crucial tool for tracking and characterizing halogenated species, enabling more accurate quantification in the subsequent studies.
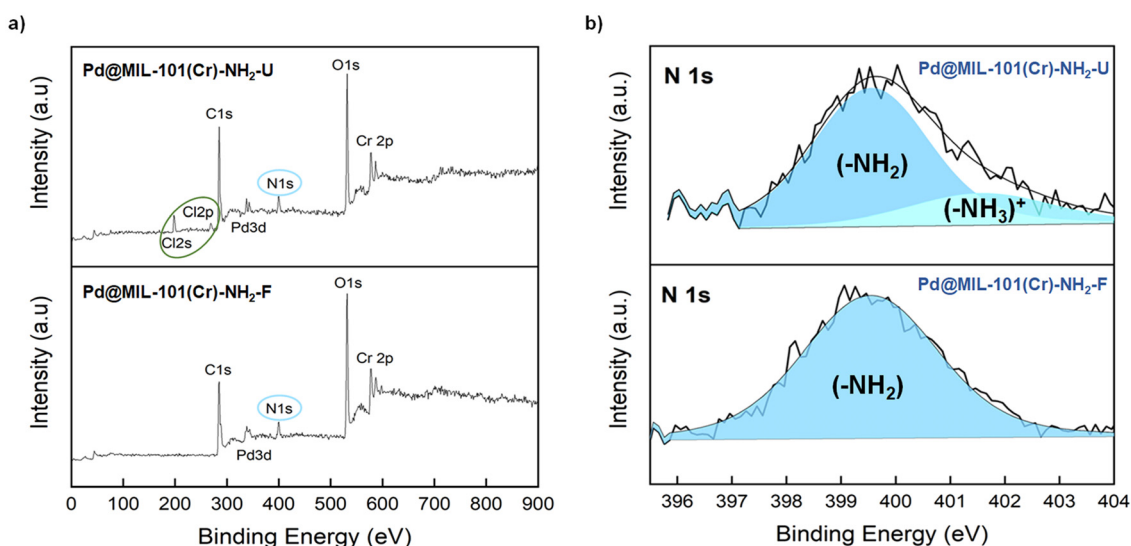

Fig. 7 XPS spectra of Pd@MIL-101(Cr)-NH$_2$ before (Pd@MIL-101(Cr)-NH$_2$-F) and after the HDH catalytic test (Pd@MIL-101(Cr)-NH$_2$-U): (a) survey and (b) N1s region.

Finally, considering that product analysis revealed no evidence of radical-type reactions (*i.e.*, absence of octane isomers, C–C coupling products, or higher oligomers) and the good mass balance closing, the HDH reaction over Pd@MIL-101 (Cr)-NH$_2$ proceeded predominantly through a Pd-heterolytic pathway rather than *via* radical intermediates.[72] The proposed mechanism is shown in Scheme 1. Initially, Pd nanoparticles (Pd^0) dissociate molecular hydrogen, generating reactive surface hydride species. The substrate 1,8-dichlorooctane then coordinates to the Pd surface, weakening the C–Cl bond. Through an oxidative addition of the C–Cl bond to Pd^0, a σ-alkyl Pd(II)–Cl intermediate palladacycle-type is formed. Subsequently, reductive elimination with a surface hydride promotes C–Cl bond cleavage and C–H bond formation, releasing 1-chlorooctane as the intermediate product and leaving Cl$^-$ adsorbed on the metal surface. In the second step, the 1-chlorooctane intermediate undergoes an analogous sequence: coordination to Pd, activation of the C–Cl bond, formation of the Pd(II)–Cl intermediate, and subsequent reduction, leading to octane as the major reaction product. Throughout this catalytic cycle, Pd^0 is continuously regenerated under a reductive atmosphere. The accumulation of chloride species, which could otherwise deactivate the metal, is mitigated through HCl formation. This HCl is captured by the amino groups of the MOF ligand (–NH$_3$$^+Cl^-$), as supported by the XPS analysis.

3.5 Reusability and regeneration

Reusability. Since the continuous reaction system employed in the catalytic tests allowed to carry out longer operational times, the lifetime under HDH conditions was assessed for Pd (4.3%)@MIL-101(Cr)-NH$_2$. Therefore, an 8-hour reaction was conducted using a feed with 1000 ppm of Cl. Fig. 8 represents the evolution of 1,8-dichlorooctane conversion and selectivity to both *n*-octane and 1-chlorooctane *versus* the reaction time. The conversion of the feed remained unaltered at 100% during
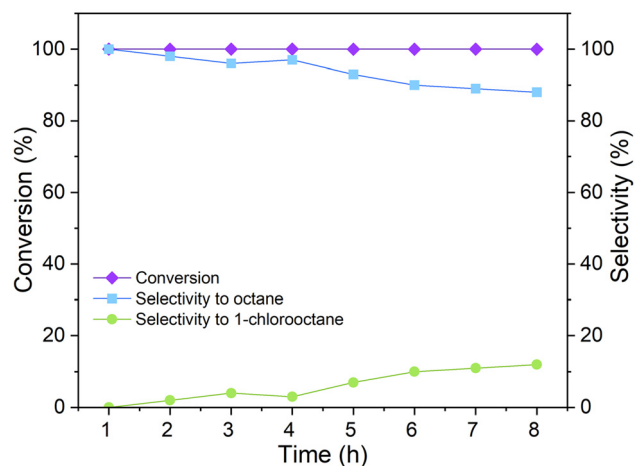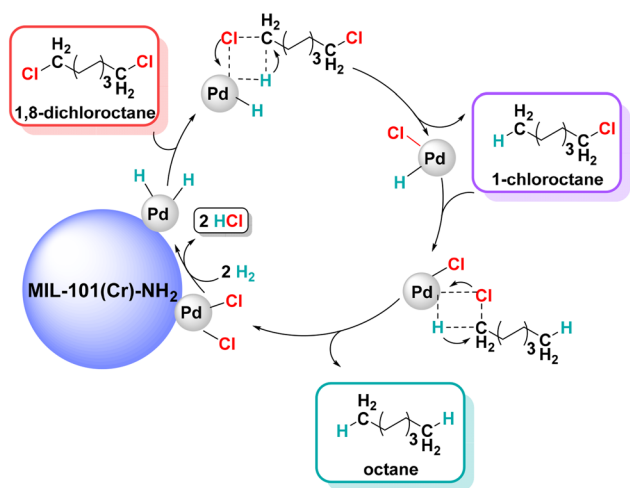

Fig. 8 Catalytic HDH of 1,8-dichloroctane: a long-term reaction test using a Pd(4.3%)@MIL-101(Cr)-NH$_2$ catalyst.

the whole experiment, while the selectivity to *n*-octane was close to 100% throughout the first 4 h of reaction followed by a slow and gradual decline, reaching 88% at the end. This slight decrease was mainly associated with the emergence of 1-chlorooctane as a partially dehalogenated intermediate.

The results showed that Pd@MIL-101(Cr)-NH$_2$ is a highly robust catalyst with excellent performance in HDH of alkyl chlorides, even during extended reaction periods. It is noteworthy that, to the best of our knowledge, this work represents one of the first studies employing a MOF-based composite under continuous-flow conditions for the challenging HDH process. Thus, just very recently, a study has been reported on the dehalogenation of dichloromethane in continuous flow over extended reaction times using a carbon nanotube-supported Pd catalyst. With that catalyst, the authors initially achieved 80% conversion of dichloromethane, but this value declined sharply around 50% after 8 h, indicating significant catalyst deactivation along the time on stream.[73]

Regeneration. In the previous section, the behavior of the catalytic system was studied over an 8-hour period. The results showed a slight decrease in selectivity towards fully dehalogenated alkanes; however, the conversion of 1,8-dichlorooctane remained constant over time. To address this matter, a regeneration of the catalyst was performed. In this procedure, after the first 8 h of the catalytic test, the used catalyst was maintained at the reaction temperature (265 °C) with a continuous flow of H$_2$ and N$_2$ for 3 h. This treatment was aimed to desorb the retained chlorine molecules, thereby clearing the catalyst's porosity and attempting to restore its selectivity and activity.

As shown in Fig. 9, after the regeneration process, its catalytic activity was fully restored. Thus, the feedstock conversion and selectivity towards the alkane were very similar to those of the fresh material for the subsequent 4 h of the reaction. It must be mentioned that the regeneration process induced a significant amount of chlorine to be desorbed from the catalyst and retained in the bubblers as HCl (0.49 mg Cl g^{-1} feed,

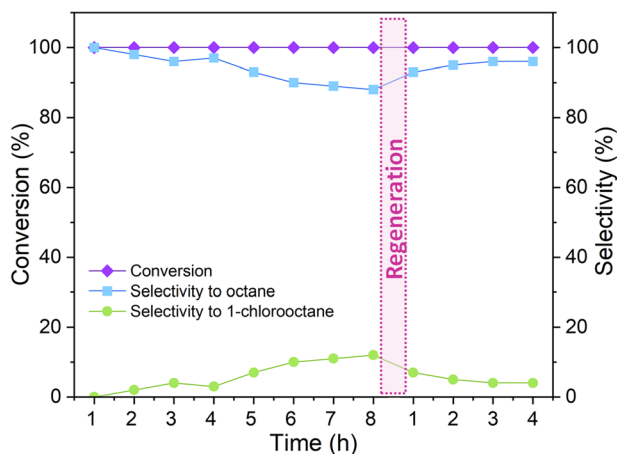**Scheme 1** Proposed mechanism for the HDH reaction of 1,8-dichloroctane catalyzed by Pd@MIL-101(Cr)-NH$_2$.

Fig. 9 Catalytic HDH of 1,8-dichlorooctane: a regeneration test maintained at 265 °C under a continuous flow of H_2 and N_2 for 3 h. The regeneration process is highlighted within the pink dotted box.

which corresponds to 15% of the total adsorbed on the MOF composite). This partial desorption of Cl can therefore be related to the restoration of the selectivity and dehalogenation capability.

The results of this study highlight the remarkable potential of the Pd(4.3%)@MIL-101(Cr)-NH_2 composite as an efficient catalyst for vapor phase HDH reactions. After 8 h of uninterrupted operation, the catalyst showed its ability to maintain 100% conversion with high dichlorination efficiency, and after a regeneration step, it fully recovered its activity and selectivity, reaching values comparable to those of the fresh catalyst over an additional 4-hour run. The dechlorination performance remained excellent, yielding an oil with minimal residual chlorine. These results highlight the robustness and reusability of the catalytic system, with negligible performance loss even after prolonged use.

4 Conclusions

This work reports for the first time the use of a composite based on Pd nanoparticles and MOFs as an efficient catalyst for the hydrodehalogenation (HDH) of 1,8-dichlorooctane, a halogenated hydrocarbon selected as a model feedstock, using a continuous fixed-bed reactor and operating under mild conditions.

A first screening process of four MOFs for the HDH of 1,8-dichlorooctane evidenced a higher catalytic activity of MOFs prepared by a microwave method (UiO-66-NH_2 and MIL-101(Cr)-NH_2) than those solvothermally synthesized (NU-1000 and MIL-100(Al)), which was attributed to their smaller particle sizes and, consequently, their improved surface-to-volume ratios and reduced diffusional constraints.

Among the two MMW-synthesized MOFs, MIL-101(Cr)-NH_2 was selected for the preparation of a theoretical 5 wt% Pd (4.3 wt% real loading) composite due to its more stable HDH

activity over time than with UiO-66-NH_2. This material was compared with a commercial 5 wt% Pd/Al_2O_3 catalyst, observing clearly superior activity with the MOF-composite (100% conversion and about 98% selectivity to *n*-octane after 4 h of reaction). TEM images of the fresh and used catalysts revealed that the improved performance was due to a better dispersion of Pd nanoparticles in the MOF, and a more effective prevention of metal agglomeration during the reaction.

Through the combination of different characterization techniques (XPS, IC and GC), it was concluded that most chlorine was retained in the MOF composite. Moreover, these Cl species could be partially removed by thermal desorption, enabling the reuse of the Pd@MOF catalyst, retaining the initial activity up to 12 h (8 h of continuous operation + 4 h after *in situ* regeneration).

In summary, the results presented here highlight the remarkable potential of the Pd(4.3%)@MIL-101(Cr)-NH_2 composite as a catalyst for vapor phase dehalogenation reactions, in different fields, such as the valorization of halogenated waste.

Author contributions

Raúl M. Guerrero: methodology and investigation & writing – original draft. Ignacio D. Lemir: supervision and writing – original draft. Sergio Carrasco: methodology and writing – review & editing. Carlos Fernández-Ruiz: methodology & investigation. David P. Serrano: conceptualization, supervision, writing – review & editing and funding acquisition. Patricia Horcajada: conceptualization, supervision, writing – review & editing and funding acquisition. Yolanda Pérez: conceptualization, supervision and writing – review & editing. Patricia Pizarro: conceptualization, supervision, writing – review & editing and funding acquisition.

Conflicts of interest

There are no conflicts of interest to declare.

Data availability

The data supporting this article have been included as part of the supplementary information (SI). Supplementary information is available. See DOI: **https://doi.org/10.1039/d5gc04671h**.

Acknowledgements

References

1 P. R. S. Kodavanti and B. G. Loganathan, in *International Encyclopedia of Public Health (Third Edition)*, ed. S. R. Quah, Academic Press, Oxford, 2025, vol. 6, pp. 204–214.

2 L. Chen, C. Zhao, X. Yuan, H. Zhang, M. Senanayake, O. Mašek, C. He and Y. S. Ok, *Green Chem.*, 2025, **27**, 4867–4897.

3 Y. Ren, H. Hu, C. Cao, G. Guo, X. Zeng, C. Zou, X. Li and H. Yao, *Waste Manage.*, 2024, **174**, 320–327.

4 J. Cueto, G. Pérez-Martín, L. Amodio, M. Paniagua, G. Morales, J. A. Melero and D. P. Serrano, *Chemosphere*, 2023, **339**, 139784.

5 T. Bhaskar, T. Matsui, J. Kaneko, M. A. Uddin, A. Muto and Y. Sakata, *Green Chem.*, 2002, **4**, 372–375.

6 M.-H. Cho, S.-H. Jung and J.-S. Kim, *Energy Fuels*, 2010, **24**, 1389–1395.

7 S. Yuan, M. Wang, B. Lv and J. Wang, *Environ. Sci. Pollut. Res.*, 2021, **28**, 9020–9028.

8 Q. Jiang, Y. Ma, P. Zhao, X. Li, Y. Shao and X. Xu, *Environ. Sci. Technol.*, 2025, **59**, 14182–14192.

9 Y. Li, J. Bu, Y. Sun, Z. Huang, X. Zhu, S. Li, P. Chen, Y. Tang, G. He and S. Zhong, *Sep. Purif. Technol.*, 2025, **356**, 129945.

10 B. R. Stanmore, *Combust. Flame*, 2004, **136**, 398–427.

11 C. Menini, C. Park, E.-J. Shin, G. Tavoularis and M. A. Keane, *Catal. Today*, 2000, **62**, 355–366.

12 P. Bhatt, M. Suresh Kumar, S. Mudliar and T. Chakrabarti, *Crit. Rev. Environ. Sci. Technol.*, 2007, **37**, 165–198.

13 R. Navon, S. Eldad, K. Mackenzie and F.-D. Kopinke, *Appl. Catal., B*, 2012, **119–120**, 241–247.

14 T. Weidlich, *Catalysts*, 2021, **11**, 1465.

15 F. Alonso, I. P. Beletskaya and M. Yus, *Chem. Rev.*, 2002, **102**, 4009–4092.

16 S. Yang, T. Guo, H. Fu, S. Zheng, J. Sun and X. Qu, *Sci. Total Environ.*, 2024, **944**, 173905.

17 G. Yuan and M. A. Keane, *J. Catal.*, 2004, **225**, 510–522.

18 J. Jeon, Y. Park and Y. Hwang, *Nanomaterials*, 2023, **13**, 1564.

19 A. Dhakshinamoorthy, M. Opanasenko, J. Čejka and H. Garcia, *Catal. Sci. Technol.*, 2013, **3**, 2509–2540.

20 V. Pascanu, G. González Miera, A. K. Inge and B. Martín-Matute, *J. Am. Chem. Soc.*, 2019, **141**, 7223–7234.

21 D. Farrusseng, S. Aguado and C. Pinel, *Angew. Chem., Int. Ed.*, 2009, **48**, 7502–7513.

22 V. I. Isaeva, O. M. Nefedov and L. M. Kustov, *Catalysts*, 2018, **8**, 368.

23 A. Felix Sahayaraj, H. Joy Prabu, J. Maniraj, M. Kannan, M. Bharathi, P. Diwahar and J. Salamon, *J. Inorg. Organomet. Polym. Mater.*, 2023, **33**, 1757–1781.

24 M. Safaei, M. M. Foroughi, N. Ebrahimpoor, S. Jahani, A. Omidi and M. Khatami, *TrAC, Trends Anal. Chem.*, 2019, **118**, 401–425.

25 L. Jiao, J. Y. R. Seow, W. S. Skinner, Z. U. Wang and H.-L. Jiang, *Mater. Today*, 2019, **27**, 43–68.

26 P. Dhumal, P. Bhadane, B. Ibrahim and S. Chakraborty, *Green Chem.*, 2025, **27**, 3815–3850.

27 Z. Sharifzadeh and A. Morsali, *Coord. Chem. Rev.*, 2022, **459**, 214445.

28 A. Valiente, S. Carrasco, A. Sanz-Marco, C.-W. Tai, A. Bermejo Gómez and B. Martín-Matute, *ChemCatChem*, 2019, **11**, 3933–3940.

29 C. Rösler and R. A. Fischer, *CrystEngComm*, 2014, **17**, 199–217.

30 L. Chen, H. Chen, R. Luque and Y. Li, *Chem. Sci.*, 2014, **5**, 3708–3714.

31 I. Lavanya, M. Nishanthan, R. Lakshmi Priya, B. S. Hariprasad, C. A. Dhayanithi and S. Ganesh Babu, *Catal. Lett.*, 2025, **155**, 73.

32 S. Luo, Z. Zeng, G. Zeng, Z. Liu, R. Xiao, M. Chen, L. Tang, W. Tang, C. Lai, M. Cheng, B. Shao, Q. Liang, H. Wang and D. Jiang, *ACS Appl. Mater. Interfaces*, 2019, **11**, 32579–32598.

33 Q. Yang, F. Yao, Y. Zhong, F. Chen, X. Shu, J. Sun, L. He, B. Wu, K. Hou, D. Wang and X. Li, *Part. Part. Syst. Charact.*, 2019, **36**, 1800557.

34 Q. Yang, Q. Xu and H.-L. Jiang, *Chem. Soc. Rev.*, 2017, **46**, 4774–4808.

35 Y. Huang, S. Liu, Z. Lin, W. Li, X. Li and R. Cao, *J. Catal.*, 2012, **292**, 111–117.

36 L. Tong, X. Song, Y. Jiang, B. Zhao and Y. Li, *Int. J. Hydrogen Energy*, 2022, **47**, 15753–15763.

37 P. Gao, Z. Hu, Y. Sheng, W. Pan, L. Ding, L. Tang, X. Chen and F. Wang, *Sci. Total Environ.*, 2024, **912**, 169572.

38 A. Carretero-Cerdán, S. Carrasco, A. Sanz-Marco, A. Jaworski and B. Martín-Matute, *Mater. Today Chem.*, 2023, **31**, 101618.

39 C. Volkringer, D. Popov, T. Loiseau, G. Férey, M. Burghammer, C. Riekel, M. Haouas and F. Taulelle, *Chem. Mater.*, 2009, **21**, 5695–5697.

40 T. E. Webber, S. P. Desai, R. L. Combs, S. Bingham, C. C. Lu and R. L. Penn, *Cryst. Growth Des.*, 2020, **20**, 2965–2972.

41 R. M. Guerrero, I. D. Lemir, S. Carrasco, C. Fernández-Ruiz, S. Kavak, P. Pizarro, D. P. Serrano, S. Bals, P. Horcajada and Y. Pérez, *ACS Appl. Mater. Interfaces*, 2024, **16**(18), 24108–24121.

42 Y. Tan, Z. Sun, H. Meng, Y. Han, J. Wu, J. Xu, Y. Xu and X. Zhang, *Appl. Organomet. Chem.*, 2020, **34**, e5281.

43 C. Volkringer, H. Leclerc, J.-C. Lavalley, T. Loiseau, G. Férey, M. Daturi and A. Vimont, *J. Phys. Chem. C*, 2012, **116**, 5710–5719.

44 A. Pankajakshan, M. Sinha, A. A. Ojha and S. Mandal, *ACS Omega*, 2018, **3**, 7832–7839.

45 B. Wan, W. Li, F. Liu, T. Lu, S. Jin, K. Wang, A. Yi, J. Tian and W. Chen, *J. Mater. Res. Technol.*, 2020, **9**, 3447–3459.

46 L. Li, Z. Li, W. Yang, Y. Huang, G. Huang, Q. Guan, Y. Dong, J. Lu, S.-H. Yu and H.-L. Jiang, *Chem*, 2021, **7**, 686–698.

47 M. L. Díaz-Ramírez, E. Sánchez-González, J. R. Álvarez, G. A. González-Martínez, S. Horike, K. Kadota, K. Sumida, E. González-Zamora, M.-A. Springuel-Huet, A. Gutiérrez-Alejandre, V. Jancik, S. Furukawa, S. Kitagawa, I. A. Ibarra and E. Lima, *J. Mater. Chem. A*, 2019, **7**, 15101–15112.

48 N. Xia, Y. Chang, Q. Zhou, S. Ding and F. Gao, *Biosensors*, 2022, **12**, 928.

49 M. S. Khan, Y. Li, D.-S. Li, J. Qiu, X. Xu and H. Y. Yang, *Nanoscale Adv.*, 2023, **5**, 6318–6348.

50 G. Férey, C. Mellot-Draznieks, C. Serre, F. Millange, J. Dutour, S. Surblé and I. Margiolaki, *Science*, 2005, **309**, 2040–2042.

51 K. Pobłocki, J. Drzeżdżon, B. Gawdzik and D. Jacewicz, *Green Chem.*, 2022, **24**, 9402–9427.

52 N. Tian, Q. Jia, H. Su, Y. Zhi, A. Ma, J. Wu and S. Shan, *J. Porous Mater.*, 2016, **23**, 1269–1278.

53 C. Qi, D. Ramella, A. M. Wensley and Y. Luan, *Adv. Synth. Catal.*, 2016, **358**, 2604–2611.

54 Y. Luan, Y. Qi, Z. Jin, X. Peng, H. Gao and G. Wang, *RSC Adv.*, 2015, **5**, 19273–19278.

55 J. M. Moreno, A. Velty and U. Díaz, *Catal. Sci. Technol.*, 2020, **10**, 3572–3585.

56 C. Ardila-Suárez, A. M. Díaz-Lasprilla, L. A. Díaz-Vaca, P. B. Balbuena, V. G. Baldovino-Medrano and G. E. Ramírez-Caballero, *CrystEngComm*, 2019, **21**, 3014–3030.

57 J. Zhou, Y. Tong, Y. He, P. Tu, B. Xue, Y. Cheng, J. Cen, Y. Zheng, J. Ni and X. Li, *Front. Chem. Eng.*, 2020, **2**, 586142.

58 Y. Zhang, C. Sun, Y. Ji, K. Bi, H. Tian and B. Wang, *Sep. Purif. Technol.*, 2024, **330**, 125293.

59 I. A. Lázaro, *Eur. J. Inorg. Chem.*, 2020, **2020**, 4284–4294.

60 H. Furukawa, U. Müller and O. M. Yaghi, *Angew. Chem., Int. Ed.*, 2015, **54**, 3417–3430.

61 C. A. Trickett, K. J. Gagnon, S. Lee, F. Gándara, H.-B. Bürgi and O. M. Yaghi, *Angew. Chem., Int. Ed.*, 2015, **54**, 11162–11167.

62 X. Ning, Y. Sun, H. Fu, X. Qu, Z. Xu and S. Zheng, *Chemosphere*, 2020, **241**, 124978.

63 R. Wojcieszak, M. J. Genet, P. Eloy, P. Ruiz and E. M. Gaigneaux, *J. Phys. Chem. C*, 2010, **114**, 16677–16684.

64 Z. Sun, W. Shi, L. R. Smith, N. F. Dummer, H. Qi, Z. Sun and G. J. Hutchings, *Nat. Commun.*, 2025, **16**, 3935.

65 H. Chen, Y. He, L. D. Pfefferle, W. Pu, Y. Wu and S. Qi, *ChemCatChem*, 2018, **10**, 2558–2570.

66 L. Tong, X. Song, Z. Hua, B. Zhao and Y. Li, *Appl. Catal., A*, 2022, **643**, 118755.

67 Q. Guan, B. Wang, X. Chai, J. Liu, J. Gu and P. Ning, *Fuel*, 2017, **205**, 130–141.

68 S. Liu, M. Martin-Martinez, M. A. Álvarez-Montero, A. Arevalo-Bastante, J. J. Rodriguez and L. M. Gómez-Sainero, *Catalysts*, 2019, **9**, 733.

69 A. Arevalo-Bastante, S. Omar, J. Palomar, M. A. Alvarez-Montero, J. Bedia, J. J. Rodriguez and L. M. Gómez-Sainero, *Chem. Eng. J.*, 2022, **446**, 136893.

70 M. Bonarowska, Z. Kaszkur, K. Matus, A. Drelinkiewicz, T. Szumełda and A. Kubas, *Chemistry*, 2021, **3**, 338–359.

71 M. Wen, G. Li, H. Liu, J. Chen, T. An and H. Yamashita, *Environ. Sci. Nano*, 2019, **6**, 1006–1025.

72 M. R. Flid, L. M. Kartashov and Y. A. Treger, *Catalysts*, 2020, **10**, 216.

73 S. Liu, A. Iglesias Juez, A. B. Hungría Hernández, M. Martín Martínez, J. Bedia García-Matamoros, J. J. Rodríguez Jiménez and L. M. Gómez Sainero, *Chem. Eng. J.*, 2024, **492**, 152128.